Mode shape transformation for model error localization with modal strain energy

Zi Huang, Chaoping Zang, Genbei Zhang, Michael I. Friswell

PII: S0022-460X(20)30061-4

DOI: https://doi.org/10.1016/j.jsv.2020.115230

Reference: YJSVI 115230

To appear in: *Journal of Sound and Vibration*

Received Date: 7 August 2019

Revised Date: 18 December 2019

Accepted Date: 30 January 2020

Please cite this article as: Z. Huang, C. Zang, G. Zhang, M.I. Friswell, Mode shape transformation for model error localization with modal strain energy, *Journal of Sound and Vibration* (2020), doi: https://doi.org/10.1016/j.jsv.2020.115230.

Mode shape transformation for model error localization with modal strain energy

Zi Huang[a], Chaoping Zang[a,*], Genbei Zhang[a], Michael I.Friswell[b]

[a] *College of Energy and Power Engineering, Nanjing University of Aeronautics and Astronautics, Jiangsu Province Key Laboratory of Aerospace Power System, Nanjing 210016, China*

[b] *College of Engineering, Swansea University, Bay Campus, Swansea SA1 8EN, UK*

CRediT author statement

Zi Huang, Chaoping Zang, Genbei Zhang, Michael I.Friswell: Conceptualization, Methodology. **Zi Huang.**: Writing- Original draft preparation. **Chaoping Zang, Michael I.Friswell::** Writing- Reviewing and Editing

Mode shape transformation for model error localization with modal strain energy

Zi Huang[a], Chaoping Zang[a,*], Genbei Zhang[a], Michael I.Friswell[b]

[a] *College of Energy and Power Engineering, Nanjing University of Aeronautics and Astronautics, Jiangsu Province Key Laboratory of Aerospace Power System, Nanjing 210016, China*

[b] *College of Engineering, Swansea University, Bay Campus, Swansea SA1 8EN, UK*

Abstract

A modeling error location method based on modal strain energy is presented in this paper. Errors in the design model with shell elements are located by an error indicator which is based on changes between the equivalent modal strain energy and the modal strain energy of the design model. The equivalent modal strain energy is defined as a quadratic form using the stiffness matrix of the design model and the mode shape of the reference coming from the sophisticated and high fidelity finite-element model, called the supermodel, or the full-field measurement. The major obstacle to obtain the equivalent modal strain energy is how to match the mode shapes of a solid element and those of a shell element since each node of the solid element contains only three translation degrees of freedom (dofs) while each node of the shell element has six dofs, including three translation and three rotation components. In order to solve this problem, a mode shape transformation method from the solid element to the shell element is proposed using the shape functions or linear approximation. Using this approach, the errors in the design model can be determined and the updating parameters can be selected so that the updated model has physical meaning and can represent the dynamic characteristics of the real structure. The simulation of a simple plate is used initially to illustrate the effectiveness of the proposed method. Then, a rotor test rig casing is taken as an example for further investigation. A comparison of the updating parameters selected by the proposed method and the traditional sensitivity analysis technique is then undertaken. It is verified that the updating parameters selected based on error location have physical sense and represent the true errors in the design model through the updating results. The advantage of this technique is that only detailed mode shapes from the reference is required. The approach shows potential for further industrial engineering applications.

Key words: Mode shape transformation, Modal strain energy, Error Indicator, Error location.

1. Introduction

In modern structural design, finite element (FE) analysis is widely used for design prediction. In general, the sophisticated and high fidelity FE model of a real structure is capable of

representing all geometric features and its dynamic properties. Therefore, this model can be taken as representative of the structure for model updating or further analysis. Such a model, also called a supermodel [1, 2], is usually created with a highly refined mesh using second-order 3D solid elements. However, the supermodel will significantly increase the number of nodes and degrees of freedom (dofs), and therefore it significantly increases the computing cost. The supermodel is also not suitable for further analysis of the whole system through assembling all sub supermodels, such as the whole engine model (WEM). Therefore, a reduced model with higher efficiency is widely used, which is called the design model. The design model is usually built with beam or shell elements and is often obtained through model reduction, including geometrical simplification or a coarse mesh, in order to significantly reduce the number of dofs in the model. These reductions will cause errors in the design model and result in a lack of agreement between the design model predictions and the reference (experimental observations or simulations from supermodels). Therefore, one of the key issues is how to localize errors in the design model and adjust the design parameters to improve the prediction accuracy of the design model using the reference data.

In recent years, correcting errors in the design model through model updating based on test data has developed into a mature technology and the details were described in references [3, 4, 5]. The updating results critically depend on the updating parameter selection strategy. Currently, most parameter selection methods are based on sensitivity analysis. Lallement et al. [6] used an iterative procedure to select the optimal subset of parameters, commonly known as the forward selection method. Friswell et al. [7, 8] examined the relationship between the subset selection and the iteration required for the parameter estimation. Linderholt et al. [9] developed a Hessian-based error localization approach to identify the updating parameters with most confidence from a set of candidates. Combining the parameters with the similarity sensitivity to improve the updating procedure was proposed by Kim et al. [10, 11, 12]. The basic idea of these methods is to select the most sensitive parameters to minimize the objective function describing the difference between the prediction and the reference. However, the most sensitive parameters may not be the erroneous parameters, and thus an updated model based on the most sensitive parameters may only be a mathematical equivalent model. The most important issue to solve the above problem is to localize the actual model errors and select the corresponding updating parameters.

The errors in the FE model arise from numerous sources and may be summarized as three types [5]: (1) discretization errors, (2) idealization errors, (3) parameter errors. Correction of the discretization and idealization errors normally occurs within the scope of model verification. After model verification, the discretization and idealization errors of design model can be assumed negligible and the design model may be used for model updating. The parameter errors of the verified design model are usually caused by inaccurate estimation within the model. Compared to the supermodel, the errors in the design model

often arise from improper simplification, particularly the simplification of detailed geometrical features. These improper simplifications can be described by stiffness or mass related parameters of the design model and can be updated. Locating these errors helps to improve the updated model fidelity and the model updating efficiency.

Error localization methods have been investigated in recent decades. Larsson and Abrahamsson [13] proposed the Balancing Eigenvalue Equation Method (BEEM) to locate model errors using the unbalanced load vector in the early days. The Best Subspace Method [13] and the Substructure Energy Function Method [14] may be considered as extensions of the BEEM approach. These methods focus on locating the errors in matrix elements or dofs, but the selected parameters lack physical meaning. The localization of error parameters in the design model is similar to structural damage detection using vibration data. The basic idea of both is to compare the modal characteristics of different states, which are damaged and undamaged states for damage detection, and the design model and reference supermodel for error localization in this paper. Doebling et al. presented a detailed review on this subject [15]. The modal strain energy (MSE) method is one of the most powerful tools and widely used in engineering because of its high sensitivity and accuracy. The principle is that the modal strain energy at the damage location area will have a significant difference before and after damage. Several typical damage indicators based on the change in modal strain energy have been proposed and can successfully detect damage or cracks in plate structures [16, 17, 18, 19, 20].

The MSE calculation depends on the accuracy of the mode shapes of the structure. The mode shapes measured using traditional accelerators are generally spatially incomplete and also lack the rotational components. The modal expansion technique could be used to expand the sparse mode data. Guyan static expansion [21] is the simplest method, which is based on the assumption that the inertial force terms for the unmeasured dofs can be ignored, although the accuracy is insufficient in many cases. Hence, the Improved Reduction System (IRS) method [22], the iterated IRS method [23] and the System Equivalent Reduction Expansion Process (SEREP) [24] have been proposed to obtain better performance. Considering that uncertainty or errors may be contained in the model, several methods have been proposed to improve the accuracy of the expanded shapes of offshore jacket structures [25, 26, 27, 28]. In addition, Guan and Karbhari [17] used polynomial functions to expand the mode shapes of beam structures. However, modal expansion will bring in extra errors and mix them with the model errors, which will increase the difficulties of error location. Another critical problem is that the measurement noise in the mode shapes also has a great influence on the modal strain energy calculation. Thus, we can use the supermodel to replace the test data to provide the reference mode shapes. Compared to the measured mode shapes, the supermodel can produce accurate mode shapes in as many dofs as required. However, there are generally only three translation dofs at each node of the supermodel, whereas there are six dofs at each node of the shell elements in the design model, including three rotational components. As a result, the

equivalent modal strain energy (EMSE) using the shell element stiffness matrix from the design model and the mode shapes from the supermodel cannot be combined easily. Thus the correct error indicator and location results cannot be obtained. For the purpose of error location using modal strain energy with the supermodel, the problem of mode shape transformation from the supermodel to the design model should be solved.

In this paper, a mode shape transformation method from the supermodel to the design model is proposed and applied to error localization based on modal strain energy. The mode shape transformation is formulated and derived based on the theory of finite element analysis using the element shape functions. An alternative transformation method with linear approximation is also proposed and discussed to simplify the transformation procedure for complex structures. An error indicator based on modal strain energy is also presented. The application of the proposed method is demonstrated by a simulated plate structure with geometrical feature simplification and the casing structure of a rotor test rig. Compared with the traditional sensitivity analysis method, it is demonstrated that the proposed method using modal strain energy and modes from the supermodel can be applied to locate the errors in the design model and guide the parameter selection in model updating.

2. Methodology

2.1 Strain energy descriptions of solid and shell elements

The flexural vibration of a flat plate structure can be modeled and analyzed by both solid and shell elements, as shown in **Fig. 1**, in the finite element method The 3D solid element consists of 8 nodes, named as 1~8. The shell element nodes are I, J, K, and L at the middle surface of the element.

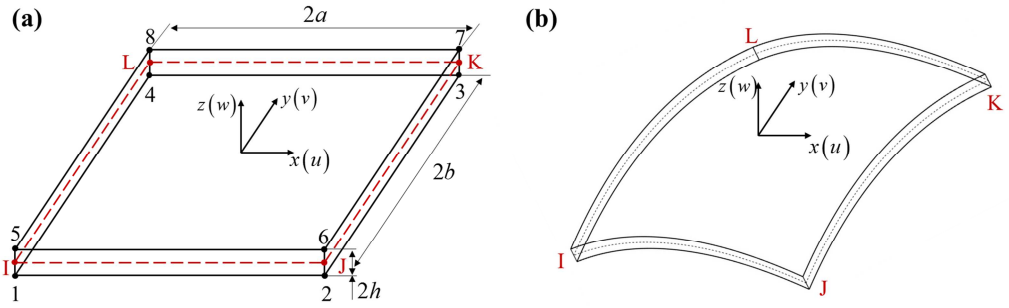

Fig. 1 The model of the flat plate (a) 3D solid element and shell element, (b) deformed plate

The strain energy expression for a finite element is

$$U = \int_V \boldsymbol{\varepsilon}^T \boldsymbol{D}\boldsymbol{\varepsilon} dV \tag{1}$$

where $\boldsymbol{D}$ is the matrix of material constants and $\boldsymbol{\varepsilon}$ is the strain component vector expressed as

$$\boldsymbol{\varepsilon} = \begin{bmatrix} \varepsilon_x & \varepsilon_y & \varepsilon_z & \gamma_{xy} & \gamma_{xz} & \gamma_{yz} \end{bmatrix}^T \tag{2}$$

The strain vector $\boldsymbol{\varepsilon}$ for a finite element can be expressed as

$$\boldsymbol{\varepsilon} = \boldsymbol{B}\boldsymbol{a} \tag{3}$$

where $\boldsymbol{B}$ is the strain matrix, and $\boldsymbol{a}$ is the displacement vector. Thus eq.(1) may be written in the form

$$U = \frac{1}{2}\int_V (\boldsymbol{B}\boldsymbol{a})^T \boldsymbol{D}(\boldsymbol{B}\boldsymbol{a})\,dV = \frac{1}{2}\boldsymbol{a}^T\left(\int_V \boldsymbol{B}^T\boldsymbol{D}\boldsymbol{B}dV\right)\boldsymbol{a} = \frac{1}{2}\boldsymbol{a}^T\boldsymbol{K}\boldsymbol{a} \tag{4}$$

where $\boldsymbol{K}$ is the element stiffness matrix. It is clear that the strain energy depends on the displacement vector. If the displacement vector is replaced by the mode shape, the element modal strain energy is given by

$$U_{i,j} = \frac{1}{2}\boldsymbol{\varphi}_j^T\boldsymbol{K}_i\boldsymbol{\varphi}_j \tag{5}$$

where i, j represent the element number and mode number respectively, and $\boldsymbol{K}_i, \boldsymbol{\varphi}_j$ are the element stiffness matrix and the mode shape vector. For the solid element, the mode shape $\boldsymbol{\varphi}_j$ can be expressed as

$$\boldsymbol{\varphi}_j = \begin{bmatrix} u_1 & v_1 & w_1 & \cdots & u_8 & v_8 & w_8 \end{bmatrix}^T \tag{6}$$

It can be seen that the mode shape of a solid element is represented by the displacement at the eight nodes and each node has three translation degrees of freedom. The shell element is the combination of a membrane element and a plate bending element and the mode shape $\boldsymbol{\varphi}_j$ is given by

$$\boldsymbol{\varphi}_j = \begin{bmatrix} u_I & v_I & w_I & \theta_{x,I} & \theta_{y,I} & \theta_{z,I} & \cdots & \theta_{x,L} & \theta_{y,L} & \theta_{z,L} \end{bmatrix}^T \tag{7}$$

Obviously, the mode shape of a shell element is described by the displacement of four nodes with six dofs at each node. These six dofs are three translational and three rotational dofs. If the mode shape of a shell element is divided into translational and rotational components

$$\boldsymbol{\varphi}_j = \begin{bmatrix} \boldsymbol{\varphi}_j^d & \boldsymbol{\varphi}_j^r \end{bmatrix} \tag{8}$$

Then, the modal strain energy of the shell element can be written in the following matrix form

$$\begin{aligned} U_{i,j} &= \frac{1}{2}\boldsymbol{\varphi}_j^T\mathbf{K}_i\boldsymbol{\varphi}_j = \frac{1}{2}\begin{bmatrix} \boldsymbol{\varphi}_j^d & \boldsymbol{\varphi}_j^r \end{bmatrix}^T \mathbf{K}_i \begin{bmatrix} \boldsymbol{\varphi}_j^d & \boldsymbol{\varphi}_j^r \end{bmatrix} \\ &= \frac{1}{2}\begin{bmatrix} \boldsymbol{\varphi}_j^d & \boldsymbol{\varphi}_j^r \end{bmatrix}^T \begin{bmatrix} \mathbf{K}_i^{dd} & \mathbf{K}_i^{dr} \\ \mathbf{K}_i^{rd} & \mathbf{K}_i^{rr} \end{bmatrix} \begin{bmatrix} \boldsymbol{\varphi}_j^d & \boldsymbol{\varphi}_j^r \end{bmatrix} \\ &= \frac{1}{2}\boldsymbol{\varphi}_j^{d,T}\mathbf{K}_i^{dd}\boldsymbol{\varphi}_j^d + \frac{1}{2}\boldsymbol{\varphi}_j^{r,T}\mathbf{K}_i^{rr}\boldsymbol{\varphi}_j^r + \frac{1}{2}\boldsymbol{\varphi}_j^{d,T}\mathbf{K}_i^{dr}\boldsymbol{\varphi}_j^r \\ &= U_{i,j}^{dd} + U_{i,j}^{rr} + U_{i,j}^{dr} \end{aligned} \tag{9}$$

where $U_{i,j}^{dd}, U_{i,j}^{rr}, U_{i,j}^{dr}$ are given as follows

$$U_{i,j}^{dd}=\frac{1}{2}\boldsymbol{\varphi}_j^{d,T}\mathbf{K}_i^{dd}\boldsymbol{\varphi}_j^{d},\quad U_{i,j}^{rr}=\frac{1}{2}\boldsymbol{\varphi}_j^{r,T}\mathbf{K}_i^{rr}\boldsymbol{\varphi}_j^{r},\quad U_{i,j}^{dr}=\frac{1}{2}\boldsymbol{\varphi}_j^{d,T}\mathbf{K}_i^{dr}\boldsymbol{\varphi}_j^{r} \tag{10}$$

If the rotation component is neglected, then the mode shape of the shell element can be written as

$$\boldsymbol{\varphi}_j=\begin{bmatrix}\boldsymbol{\varphi}_j & \boldsymbol{0}\end{bmatrix} \tag{11}$$

Substituting eq.(11) into eq.(10), the energies $U_{i,j}^{rr},U_{i,j}^{dr}$ are equal to zero and

$$U_{i,j}\left(\begin{bmatrix}\boldsymbol{\varphi}_j^{d} & \boldsymbol{0}\end{bmatrix}\right)=U_{i,j}^{dd},\quad \left(U_{i,j}^{rr}=0,U_{i,j}^{dr}=0\right) \tag{12}$$

Setting the rotation component to zero is equal to applying fixed constraints to these dofs. According to the virtual work principle, these added constraints will increase the structure's ability to resist deformation and more energy is required to generate same deformation, which means the modal strain energy without considering rotation component will be larger than the real value

$$U_{i,j}\left(\begin{bmatrix}\boldsymbol{\varphi}_j^{d} & \boldsymbol{0}\end{bmatrix}\right)>U_{i,j}\left(\begin{bmatrix}\boldsymbol{\varphi}_j^{d} & \boldsymbol{\varphi}_j^{r}\end{bmatrix}\right) \tag{13}$$

The same conclusion could be drawn for the translation dofs, as

$$U_{i,j}\left(\begin{bmatrix}\boldsymbol{0} & \boldsymbol{\varphi}_j^{r}\end{bmatrix}\right)>U_{i,j}\left(\begin{bmatrix}\boldsymbol{\varphi}_j^{d} & \boldsymbol{\varphi}_j^{r}\end{bmatrix}\right) \tag{14}$$

Because the modal strain energy is positive, the cross terms $U_{i,j}^{dr}$ are negative and the modal strain energy of all components can be expressed as the algebraic sum

$$U_{i,j}=U_{i,j}^{dd}+U_{i,j}^{rr}-\left|U_{i,j}^{dr}\right| \tag{15}$$

Fig. 2 shows a typical comparison of the modal strain energy components of the shell elements of a plate using a logarithmic scale. It clearly shows that the modal strain energy components $U_{i,j}^{dd},U_{i,j}^{rr},\left|U_{i,j}^{dr}\right|$ are orders higher than the correct value $U_{i,j}$. The results mean that the rotational components of the mode shape of shell elements have a great influence on the modal strain energy.

Note that, in practice, if the rotational dofs were not measured they would not simply be neglected, and the element stiffness matrices in the design model could be reduced to only the translational dofs using the IRS method or the iterated IRS technique.

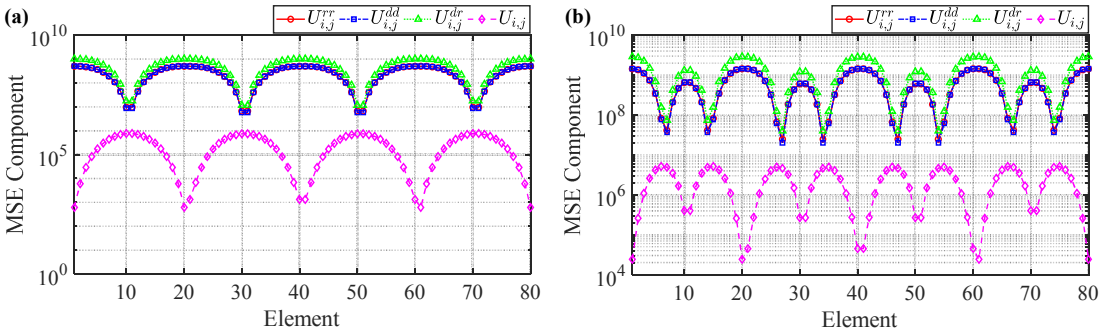

Fig. 2 Typical comparison of modal strain energy components of shell elements of a plate, (a) the 1st

mode, (b) the 2nd mode

2.2 Mode shape transformation from a solid element to a shell element

Taking the element in **Fig. 1** as an example, the translational mode shape at any location in the solid element can be described using the shape functions in the x, y, z-directions as

$$u=\sum_{i=1}^{8}N_i u_i,\quad v=\sum_{i=1}^{8}N_i v_i,\quad w=\sum_{i=1}^{8}N_i w_i \tag{16}$$

where N_i are the shape functions of the solid element. Thus, the translational elements of the mode shape at nodes I, J, K, L of the shell element can be obtained as

$$u_p=\sum_{i=1}^{8}N_i(p)u_i,\quad v_p=\sum_{i=1}^{8}N_i(p)v_i,\quad w_p=\sum_{i=1}^{8}N_i(p)w_i,\quad p=I,J,K,L \tag{17}$$

According to the finite element theory of shell elements, there are only two out-of-plane rotational dofs in the elemental coordinate system. The in-plane rotational dof is used for coordinate transformation and doesn't make physical sense in element coordinate system. The relationship between the normal translation w and the rotations θ_x,θ_y of the shell element are

$$\theta_x=\frac{\partial w}{\partial y},\quad \theta_y=-\frac{\partial w}{\partial x} \tag{18}$$

However, the polynomial function degree of the normal translation w of the solid element is less than the polynomial function degree of the shell element. The direct calculation using the partial derivative of the normal translation within the solid element is not accurate enough. According to the assumption of shell element theory [29], the translation of the shell element parallel to the undeformed middle surface is given by

$$u=-z\frac{\partial w}{\partial x},\quad v=-z\frac{\partial w}{\partial y} \tag{19}$$

Combining eq.(18) and eq.(19), the rotations θ_x,θ_y can be expressed as

$$\theta_x=-\frac{v}{z},\theta_y=\frac{u}{z} \tag{20}$$

Clearly the rotations θ_x,θ_y could be obtained through the quotient of the translation along the z-direction, which represents the slope of translation change along the normal direction. Therefore, these slopes can be expressed as the partial derivatives

$$\theta_x=-\frac{\partial v}{\partial z},\theta_y=\frac{\partial u}{\partial z} \tag{21}$$

Substituting eq.(17) into eq.(21), the rotational components of the mode shapes at nodes I, J, K, L in the plate element can be expressed as

$$\begin{cases} \theta_{x,p} = -\dfrac{\partial\left(\sum_{i=1}^{8} N_i(p) v_i\right)}{\partial z} = -\sum_{i=1}^{8} \dfrac{\partial N_i(p)}{\partial z} v_i \\ \theta_{y,p} = \dfrac{\partial\left(\sum_{i=1}^{8} N_i(p) u_i\right)}{\partial z} = \sum_{i=1}^{8} \dfrac{\partial N_i(p)}{\partial z} u_i \end{cases} \quad p = I, J, K, L \tag{22}$$

The above derivation defines the process of mode shape transformation from the solid elements to the shell elements via the shape functions, where eq.(17) and eq.(22) give the components of the equivalent mode shape.

Actually, the computation procedure and the derivative of the shape function are both complicated and time consuming, especially for irregular high order hexahedron elements. If the thickness parameter h of the shell element is thin enough, the linear approximation method could be used as an alternative to obtain the mode shapes at nodes I, J, K, L and simplify the transformation procedure. For example, the mode shape at node I are given by

$$u_I = \frac{u_1 + u_5}{2} \quad v_I = \frac{v_1 + v_5}{2} \quad w_I = \frac{w_1 + w_5}{2} \quad \theta_{x,I} = -\frac{v_5 - v_1}{2h} \quad \theta_{y,I} = \frac{u_5 - u_1}{2h} \tag{23}$$

Because the mode shape transformation process is within the elemental coordinate system, it needs to be transformed to the global coordinate system using the direction cosine matrix. All the derivations above are based on the basic principles and assumptions of the finite element method, and so the transformation method can be extended to all kinds of shell elements.

2.3 Error indicator based on modal strain energy

The characteristic equation for the design model can be expressed as

$$(\boldsymbol{K} - \lambda \boldsymbol{M})\boldsymbol{\varphi} = \boldsymbol{0} \tag{24}$$

where $\boldsymbol{K}$ and $\boldsymbol{M}$ are the stiffness matrix and mass matrix, respectively, and $\lambda, \boldsymbol{\varphi}$ are the eigenvalue and eigenvector of the design model, respectively. The mass distribution of the design model can be checked by comparing with that of the supermodel and the mass parameters tuned to make them consistent with the supermodel. It is reasonable that the errors in the mass distribution of the design model could be considered as negligible after the mass tuning procedure. The characteristic equation of the reference supermodel can be expressed as

$$(\boldsymbol{K}^* - \lambda^* \boldsymbol{M}^*)\boldsymbol{\varphi}^* = \boldsymbol{0} \tag{25}$$

where $\boldsymbol{K}^*$ is the stiffness matrix of supermodel, $\boldsymbol{M}^*$ is the mass matrix, and $\lambda^*, \boldsymbol{\varphi}^*$ are the eigenvalue and eigenvector of the supermodel respectively. With reference to the strain energy damage indictor, the error indicator can be defined as

$$\chi_{i,j} = \frac{U_{i,j}^E - U_{i,j}}{U_{i,j}} \tag{26}$$

where $U_{i,j}$ represents the modal strain energy of the i^{th} element of the j^{th} mode of the

design model. $U_{i,j}^{E}$ represents the equivalent modal strain energy of the i^{th} element of the j^{th} mode, and can be written as

$$U_{i,j}^{E} = \frac{1}{2}\boldsymbol{\varphi}_j^{E,T}\boldsymbol{K}_i\boldsymbol{\varphi}_j^{E} \tag{27}$$

where the equivalent mode shapes, $\boldsymbol{\varphi}_j^{E}$, are extracted from the reference mode shapes, $\boldsymbol{\varphi}_j^{*}$, using the mode shape transformation method. $\boldsymbol{K}_i$ is the stiffness matrix of the i^{th} element of the design model. Because the error in the model will cause all of the terms in the mode shapes to change, the equivalent mode shape of those elements without errors are still slightly different from the mode shape of corresponding design model. Therefore, none of the error indicators of the design model elements are exactly zero. In order to determine the elements with real errors, a normalized error indicator is defined as

$$\eta_{i,j} = \frac{\left|\chi_{i,j} - \bar{\chi}_j\right|}{\sigma_{\chi,j}} \tag{28}$$

where $\bar{\chi}_j, \sigma_{\chi,j}$ represent the mean value and the standard deviation of indicator for the j^{th} mode and are given by

$$\bar{\chi}_j = \frac{1}{n}\sum_{i=1}^{n}\chi_{i,j}, \quad \sigma_{i,j} = \sqrt{\frac{1}{n-1}\sum_{i=1}^{n}\left(\chi_{i,j} - \bar{\chi}_j\right)^2} \tag{29}$$

Furthermore, a criterion can be set that the normalized indicator should be larger than 2, which means the confidence of the error is real is larger than 0.95. Then, small indicator errors are truncated since the corresponding elements do not contain real error. Thus

$$\eta_{i,j} = 0 \quad if \quad \left|\eta_{i,j}\right| < 2 \tag{30}$$

For some particular modes, the elements in error may be located in a position that is very insensitive to the strain energy, such as the nodal line area, and the error indicator may not be able to indicate its position. Therefore, all of the m modes of concern should be considered, and the combined normalized error indicator for the i^{th} element is defined as

$$\bar{\eta}_i = \frac{1}{m}\sum_{j=1}^{m}\eta_{i,j} \tag{31}$$

In a summary, the process of error localization based on modal strain energy consists of three steps, as shown in **Fig. 3**. The first step is to establish the supermodel and the design model and extract the model data information. Then, the next step is to offset the nodes of the design model by half the thickness of each element and establish virtual elements, as shown at the left of step 2 in **Fig. 3**, and determine the mode shape transformation from the supermodel to the design model using the proposed method. The modal strain energy and the equivalent modal strain energy are then calculated. The error indicators then enable the updating parameters to be selected based on the localization results. Finally, model updating using sensitivity analysis is performed and the updating results evaluated.

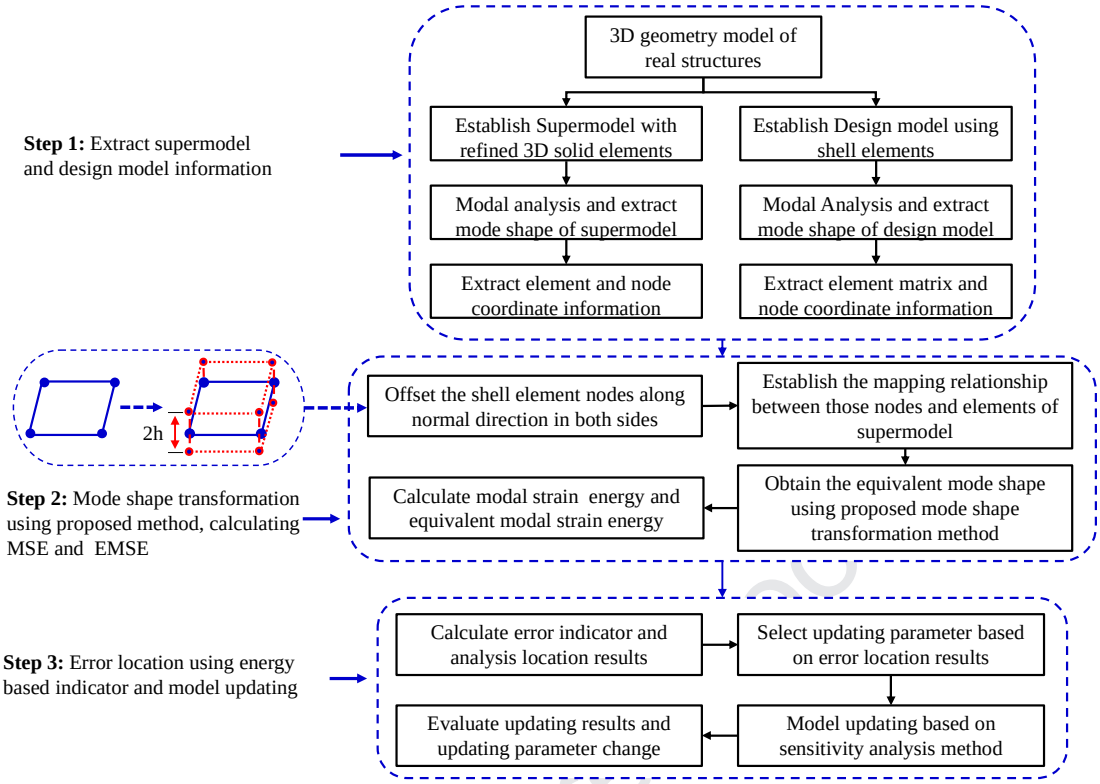

Fig. 3 The block diagram of error localization based on modal strain energy and model updating

3. Numerical Case Study

To verify the proposed method, a numerical example of plate structure with multiple errors is studied to demonstrate the effectiveness. All the simulations are calculated by the finite element analysis code MSC.NASTRAN and processed using MATLAB.

3.1 Finite element model

A rectangular plate structure with length 100mm, width 20mm and thickness 2mm is shown in **Fig. 4** (a), with small boss and notch features of size 3x3x1 mm in the structure. The material properties are those of aluminum with an elastic modulus of E=79GPa, a mass density of ρ=2700kg/m^3, and a Poisson's ratio of μ=0.3. The supermodel was created by 20-node second-order hexahedral elements with a mesh size of 1×1×1mm. The design model was created with 8-node second-order shell elements with a size of 5mm and a total of 80 elements, as shown in **Fig. 4** (b). The boss and notch features are modelled in the supermodel, but not in the design model. By comparison with supermodel, the error due to the boss is located in the 3rd element of the design model and the error due to the notch is located in the 57th element. The first five modes of the supermodel and the design model are used to demonstrate the procedure of error location, and the mode shapes of the design model are shown in **Fig. 5**. The 1st, 2nd and 4th modes are the first three bending modes in the z-direction, and the 3rd and 5th modes are the first and second torsional modes.

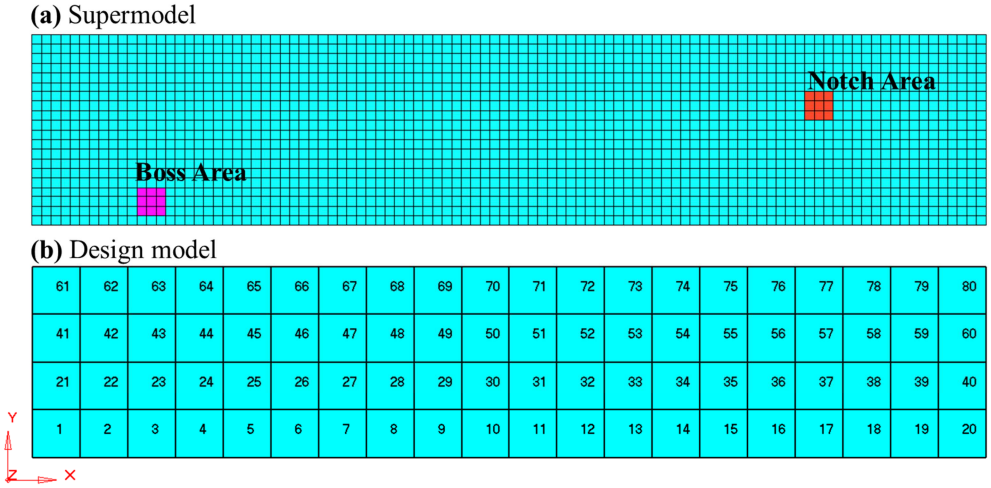

Fig. 4 Finite element models of the plate, (a) Supermodel, (b) Design model

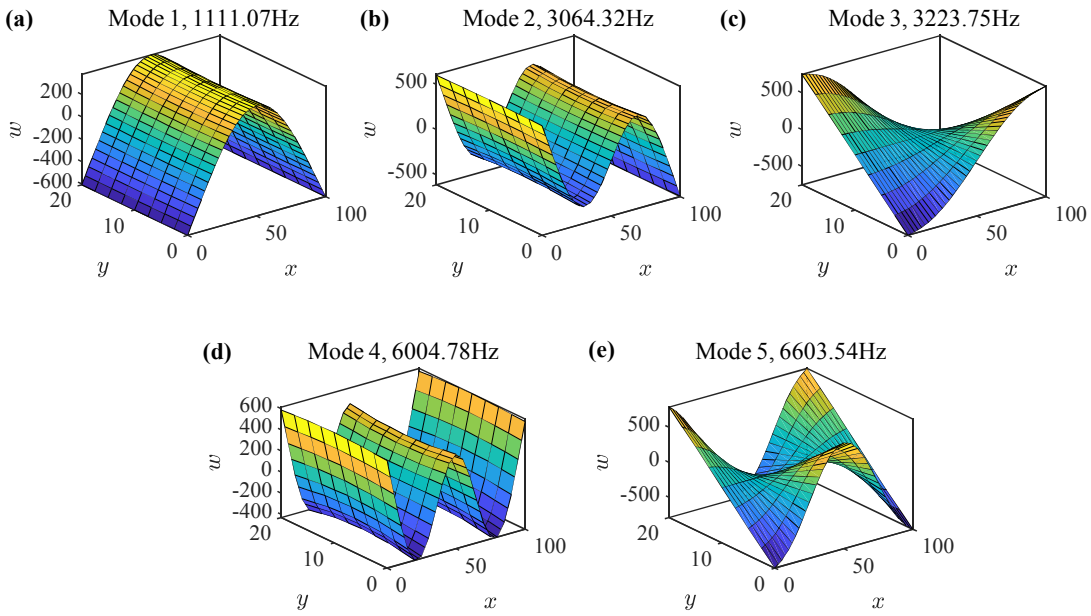

Fig. 5 First five mode shapes of the design model of the plate, (a) the 1st mode, (b) the 2nd mode, (c) the 3rd mode, (d) the 4th mode, (e) the 5th mode

3.2 Mode shape transformation using the shape function method and error location

In order to locate the errors in the design model, the mode shape transformation from the supermodel to the design model and the equivalent modal strain energy should be calculated first. Following the error localization process described in **Fig. 3**, the equivalent mode shape from the supermodel and the equivalent modal strain energy are obtained at the first and second steps. First, the node coordinate information is extracted from both models. Then, the nodes of the design model are offset by half of the thickness, $h = 1.0mm$, along the normal direction and coordinates of these nodes are extracted, as shown in **Fig. 3**. These nodes are then projected onto the supermodel, via a virtual solid element, and the mapping relationship

between these nodes and those of elements of the supermodel is established. Next, the three translational components of the equivalent mode shape of these nodes using the shape function of the supermodel element is determined. The rotational components of the equivalent mode shape are calculated by the partial derivatives of the shape functions of the virtual element. Finally, the equivalent modal strain energy of every element for each mode can be calculated using the equivalent mode shape and the element stiffness matrix of the design model. The pseudocode for the whole procedure to calculate the modal strain energy and the equivalent modal strain energy is given in **Fig. 6**.

1. **Initialize**
   (a) Supermodel and design model modal analysis;
   (b) Nastran output file: *.becho*, *.f06* from suermodel; *.becho*, *.f06, .op2*, *.op4* from design model;
2. **Extract model information about supermodel and design model**
   (a) Extract element, node data from *.becho* file, mode shape data from *.f06* file. Supermodel data: ***snode, selem, sphi*** ; design model data: ***dnode, dphi***;
   (b) Extract stiffness matrix ***Ke*** from *.op4* file, direction cosine matrix ***lamda*** from *.op2* file and obtain coordinate transform matrix ***T***;
   (c) Calculate global stiffness matrix ***Kg=T'*Ke*T***;
3. **Design model node offset both sides along normal direction, *h=1.0mm***
   (a) Virtual Top node, ***dnode_top***; Virtual bottom node, ***dnode_bot***;
4. **Node project and establish the map relationship between *dnode, dnode_top, dnode_bot* and *selem***
   (a) while *i*< number of ***dnode;*** find ***dnode***(*i*) in which element in ***selem,*** get map data ***dnode_prj;*** end
   (b) Repeat ***dnode_top*** and ***dnode_bot***, get ***dnode_top_prj***, ***dnode_bot_prj***
5. **Calculate equivalent mode shape**
   (a) Calculate the shape function ***SN*** of ***selem*** based on ***dnode_prj,*** extract u^E, v^E, w^E of equivalent mode shape ***ephi*** using ***SN*** and ***sphi*** based on eq.(17);
   (b) Repeat ***dnode_top***, ***dnode_bot*** above;
   (c) Using ***dnode***, ***dnode_top*** and ***dnode_bot*** to establish the virtual element ***velem*** data;
   (d) Calculate the shape function ***VSN*** of ***velem*** and its partial against *z* using eq.(22), get θ^x and θ^y of ***ephi;***
6. **Calculate the modal strain energy and equivalent modal strain energy**
   (a) Modal strain energy ***mse, mse=1/2*dphi'*Kg*dphi;***
   (b) Equivalent modal strain energy ***emse, emse=1/2*ephi*Kg*ephi;***

Fig. 6 The pseudocode of the analysis procedure to calculate the modal strain energy and the equivalent modal strain energy

The comparison of the equivalent modal strain energy and the modal strain energy of the design model for the first five modes are plotted in **Fig. 7**. It clearly shows that the equivalent modal strain energies are different from the modal strain energy of the design model, especially at those elements in error and the adjacent elements. There are also some deviations for other elements, such as those elements near elements 30 and 50 for the 3rd mode and elements 35 and 55 for the 5th mode. These deviations are caused by the influence of model error with different element types. In these modes, the absolute difference for these elements are significantly larger than the deviations for the 3rd element. However, these elements are not the elements with physical errors. The 3rd and 5th modes are torsional modes which causes errors in the element formulation which are particularly noticeable for elements with high strain energy in twisting motion. This makes the absolute sensitivity of the modal strain energy of these elements for these two modes to be much higher than for the 3rd element. Thus, the relative change is preferred as an error indicator rather than the absolute difference. Obviously, the relative changes at these elements are much smaller than those for the

elements with real errors. The error indicators, χ, for the first five modes are shown in **Fig. 8**, and it clearly shows that error indicators for the 3rd and 57th elements stand out from the others. The negative indicator value of the 3rd element indicates that the stiffness of that area of the supermodel is larger than the design model because of a boss in the 3rd element. Similarly, due to the notch feature, the indicator value of the 57th element is positive.

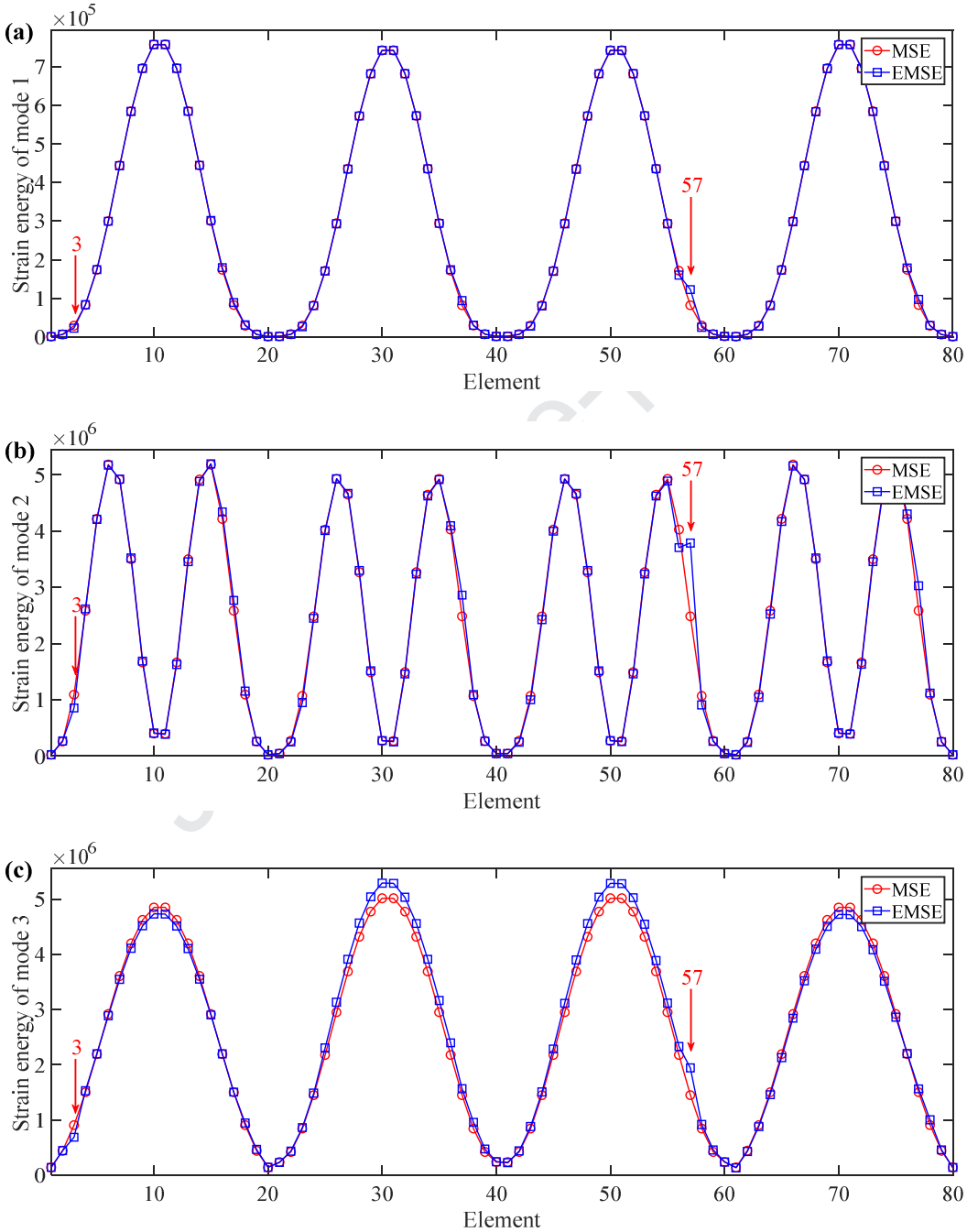

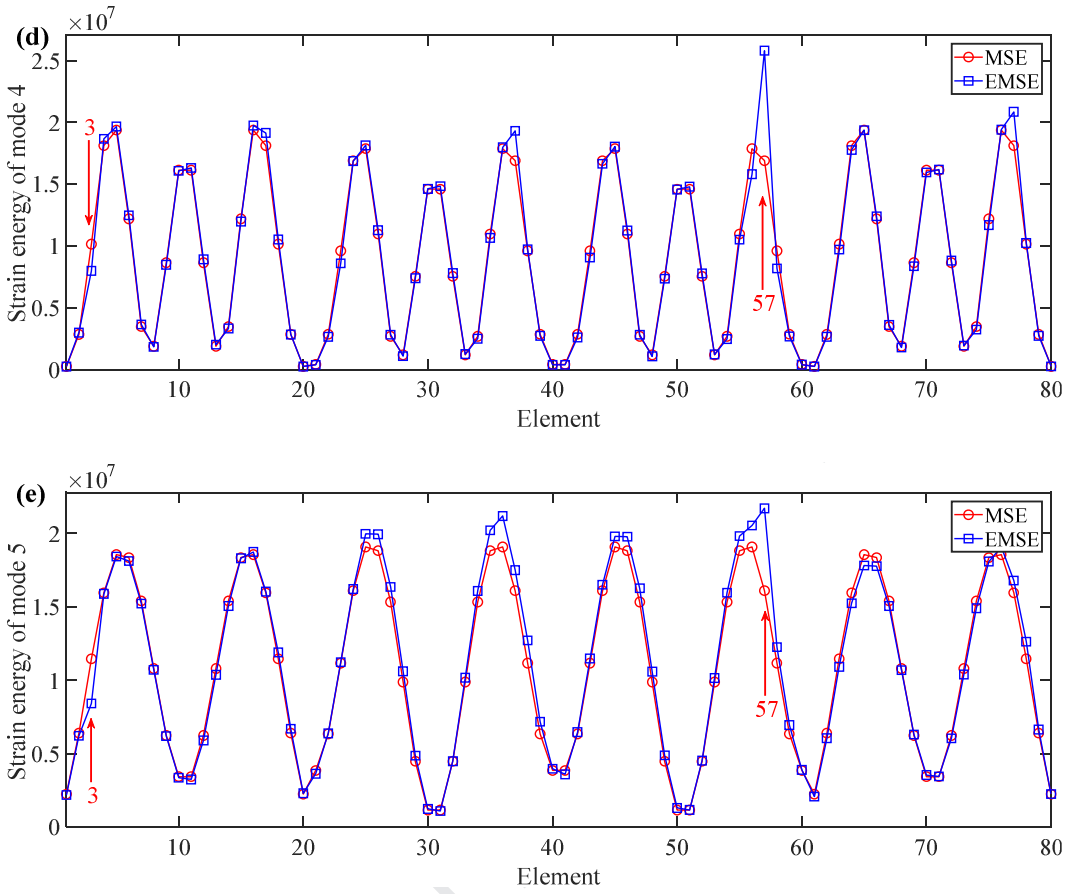

Fig. 7 The comparison of modal strain energy (MSE) and equivalent modal strain energy (EMSE) for the plate example, (a) the 1st mode, (b) the 2nd mode, (c) the 3rd mode, (d) the 4th mode, (e) the 5th mode

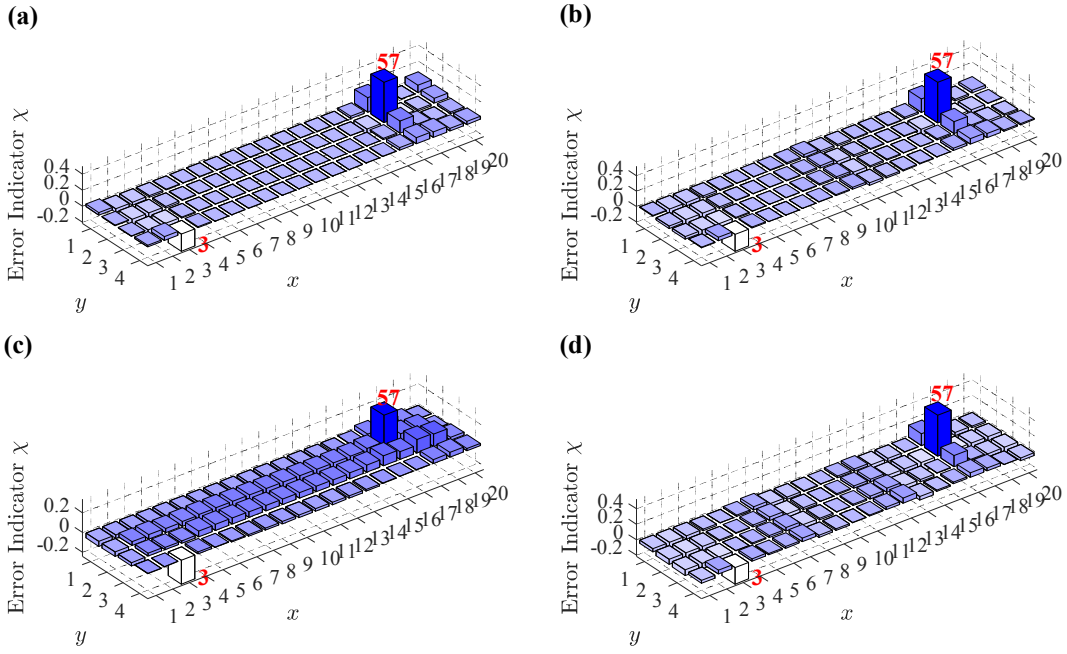

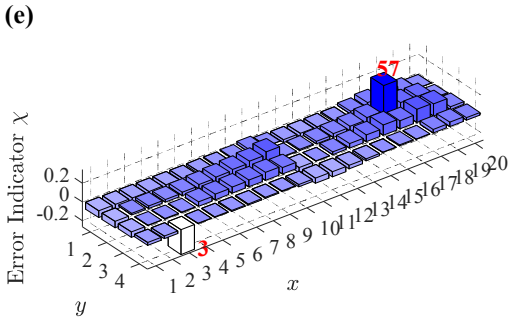

Fig. 8 Error indicators for the first five modes of the plate example, (a) the 1st mode, (b) the 2nd mode, (c) the 3rd mode, (d) the 4th mode, (e) the 5th mode

In order to eliminate the non-physical error indicators for the elements, the normalized and truncated indicators for the first five modes are used, and the combined error indicators are shown in **Fig. 9**. The results in **Fig. 9** (a) ~ (e) show that these normalized indicators for the first five modes can correctly locate the errors to the 3rd and 57th elements, with a boss and notch feature respectively. The first mode indicator gives a false result at the 77th element since the notch influences the mode shape amplitudes of all nodes of element 57, and the elements sharing nodes with element 57 will be affected. The combined indicator for all five modes, shown in **Fig. 9** (f), clearly reveals the location of the protrusion at the 3rd element and the notch at the 57th element. The indicator value of the boss element is significantly less than the notch element. This is because the stiffness change caused by the notch is much bigger than the effect of the boss feature. The localization results show that the mode shape transformations are correct and may be used for error location.

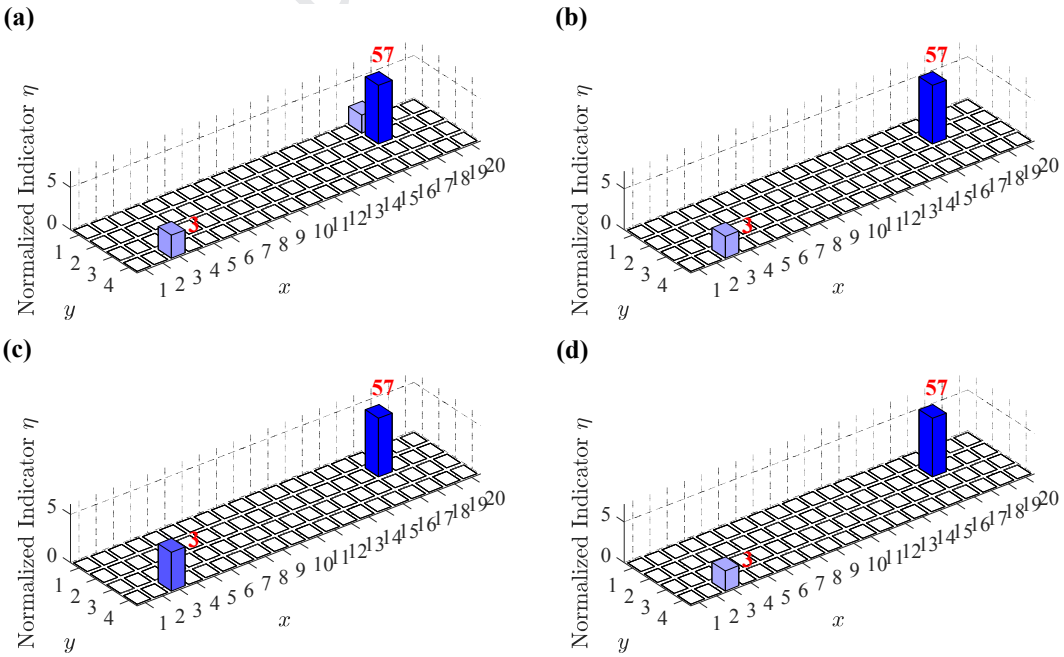

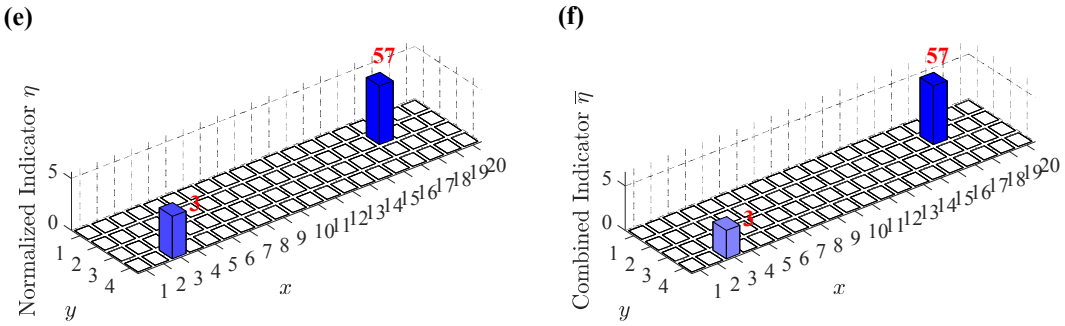

Fig. 9 Normalized error indicators for the first five modes of the plate example and combined using the shape function method, (a) 1st mode, (b) 2nd mode, (c) 3rd mode, (d) 4th mode, (e) 5th mode, (f) Combined Error Indicator for the first five modes

3.3 Verification of the linear approximation method

The shape function method has been proved to be accurate for mode shape transformation. However, the time and cost of computation will grow rapidly for larger and complex models. Compared with the shape function method, the linear approximation method can simplify the transformation process and improve the efficiency. But the accuracy of this method should be checked further. Compared to the equivalent modal strain energy using the shape function method, the deviation of the equivalent modal strain energy according to the linear approximation method are plotted in **Fig. 10**. The errors in strain energy for the elements located at the left and right edge of the plate are higher because the energies are very small and the numerical error caused by the approximation makes the deviation larger. But overall, the maximum deviation for all of the elements is 1.10% in the fourth mode. These results show that the linear approximation method retains high accuracy and can be applied as an alternative to the shape function method.

The normalized and truncated error indicators based on the equivalent modal strain energy using the linear approximation method are plotted in **Fig. 11**. Obviously, the localization results based on the linear approximation method can correctly locate the modeling errors. Therefore, the mode shape transformation based on the linear approximation will be used for the following example of the error localization in large and complex casing structures.

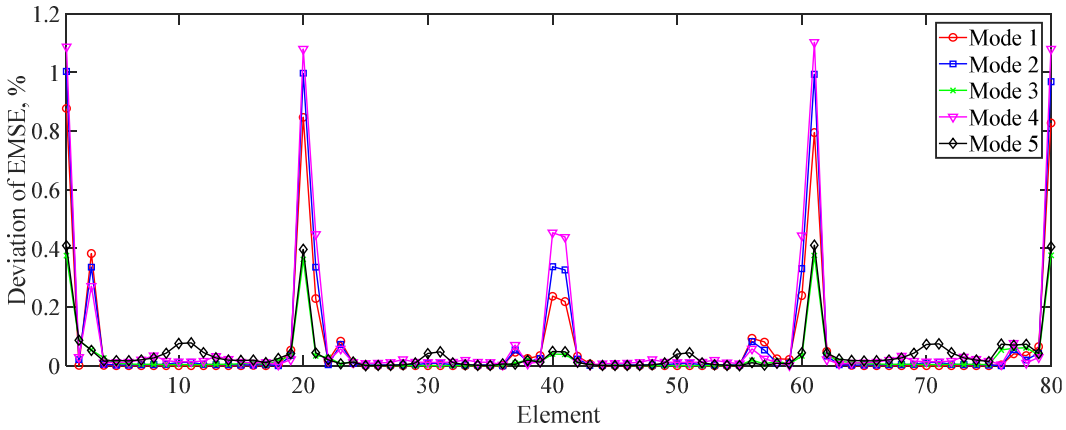

Fig. 10 The deviation of equivalent modal strain energy between linear approximation and shape function methods

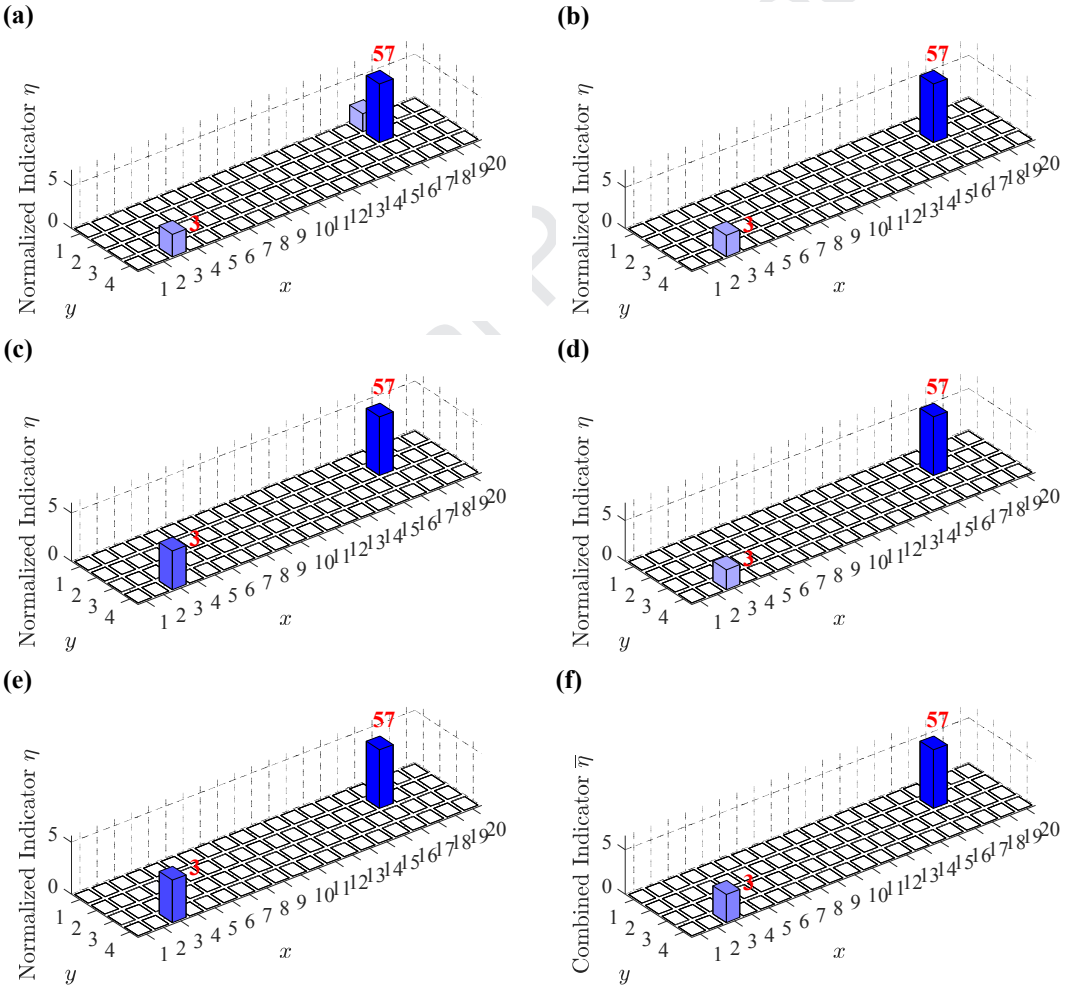

Fig. 11 The normalized and truncated error indicators for the first five modes of the plate example and combined using the linear approximation method, (a) 1st mode, (b) 2nd mode, (c) 3rd mode, (d) 4th mode, (e) 5th mode, (f) Combined Error Indicator for the first five modes

4. Experimental case study

4.1 Description of the experiment

To demonstrate the application of the error location method in an engineering example, a casing structure of a test rig was tested. The casing structure and experimental setup is shown in **Fig. 12**(a). There are eight bolt holes in both flanges and a small protrusion feature with a through hole for lubrication near the upper (corresponding to the left flange in the mode shape figures) flange. The modal test of the casing was conducted with two accelerometers and hammer excitation using SIMO (Single -Input and Multiple -Output) method. Four elastic ropes were tied to four bolt holes of the upper flange to simulate the free-free boundary condition. The casing was divided into a grid of 16×6 measurement points. The first and last set of measurement points around the casing were located at the flanges and the other four sets were located on the outer face of the casing. Because the casing is approximately axisymmetric, the frequencies of the repeated nodal diameter modes will be very close. Therefore, two accelerometers were bonded to the structure in the circumference direction at an angle to identify the repeated modes. A PCB hammer was used to provide the impulse force. The roving excitation and fixed response signals were collected by a four channel data acquisition system. Three averages were used to enhance the data accuracy and the final frequency response functions (FRFs) were calculated. Modal analysis was performed using ICATS and the modal characteristics were obtained. The first ten modes are shown in **Fig. 13**.

Due to the limitation of the experimental measurement points and locations, the complete mode shape data at all nodes is difficult to obtain. A supermodel without any geometric simplification was used as an alternative to provide the reference mode shape data and the supermodel was validated through the modal test. The modal frequency error and MAC value were used to evaluate the similarity between the prediction results of the supermodel and the test results. In general, if the modes within the frequency range of interest of the two models can be paired one by one, the MAC values of the paired modes is greater than 0.80 and the frequency error is less than 2.0%. Then, the supermodel could be used as an alternative of the experimental data to provide reference data for model updating or other purposes.

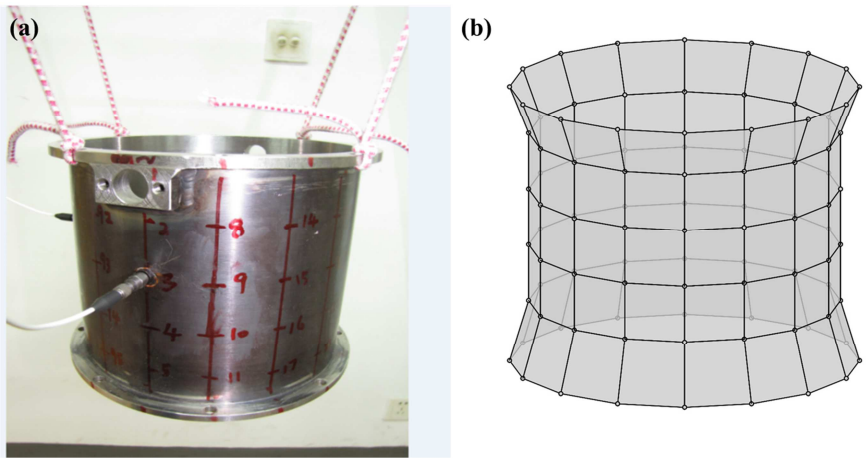

Fig. 12 Experimental configuration of the casing, (a) Experimental setup, (b) Measurement points

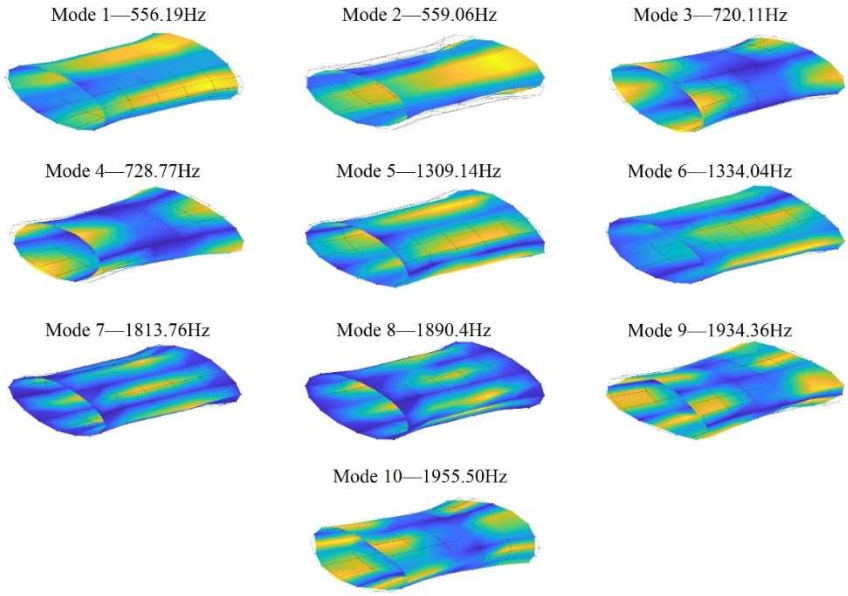

Fig. 13 The first ten mode shapes of the casing

4.2 Finite element analysis

The supermodel and design model are shown in **Fig. 14**. The material properties are taken from stainless steel where the elastic modulus is E=197GPa, the mass density is ρ=7900kg/m^3, and Poisson's ratio is μ=0.24. There are more than 70,000 elements and 140,000 nodes in the supermodel, but the design model only has 240 elements and 768 nodes in total. The predicted natural frequency errors and the MAC between the analysis and the test results are shown in **Table 1**. Correlation results for the first ten modes between the supermodel and the test show a close agreement; the maximum frequency error is 1.45% and the MAC values are larger than 0.82. The results show the supermodel can provide accurate predictions and can be used as an alternative to the test data.

Compared to the supermodel, the design model, with the bolt holes and protrusion removed, is built with shell elements. The red and blue parts are the left and right flanges

respectively. The four elements with a dark green color represent the protrusion feature area approximately, and have been initially assigned the same stiffness property as the other elements of the cylinder part. The correlation results between the design model and the test data show that the frequency errors for most modes are larger than 3.77% and up to 8.92% for the first mode, and the MAC values for all ten modes are larger than 0.79. The natural frequency errors are larger than engineering requirements and some incorrect parameters of the design model should be updated to reduce these errors.

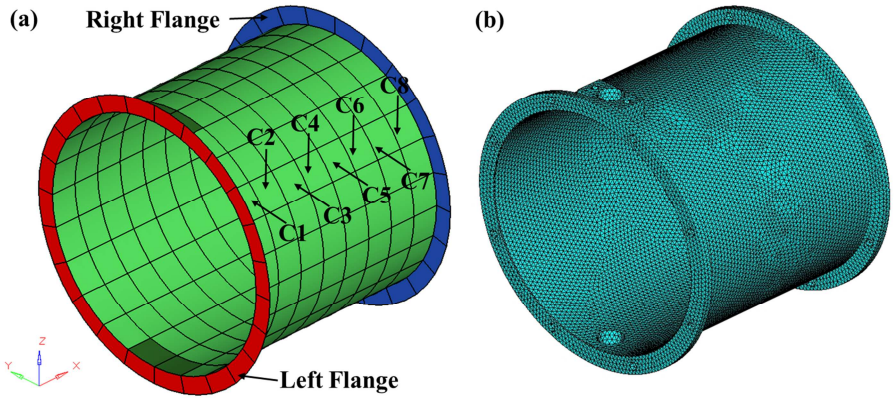

Fig. 14 Finite element model of the casing, (a) Design model, (b) Supermodel

Table 1
Predicted natural frequencies and errors between the finite element models and the test data

Mode	Test/Hz	Supermodel			Design Model		
		FEM/Hz	Error/%	MAC	FEM/Hz	Error/%	MAC
1	556.19	558.59	0.43	0.82	605.82	8.92	0.79
2	559.06	566.29	1.29	0.84	605.82	8.36	0.83
3	720.11	719.60	-0.07	0.83	763.82	6.07	0.81
4	728.77	737.33	1.18	0.89	763.82	4.81	0.87
5	1309.14	1328.14	1.45	0.91	1421.84	8.61	0.89
6	1334.04	1348.07	1.05	0.88	1421.84	6.58	0.87
7	1813.76	1829.93	0.89	0.95	1882.21	3.77	0.92
8	1890.41	1871.64	-0.99	0.93	1882.22	-0.43	0.88
9	1934.36	1938.89	0.23	0.93	2059.24	6.46	0.96
10	1955.5	1972.90	0.89	0.92	2059.24	5.31	0.84

4.3 Parameter selection with error location method and sensitivity analysis

The objective of the error location is to identify the design model errors and select updating parameters within the identified regions. In order to reduce the number of parameters and provide more physical meaning, ten substructures are defined first and the symmetry of the model is preserved as much as possible. These substructures are the left

flange (LF), the right flange (RF) and eight components of the cylinder part along the axial directions (C1, C2, … ,C8), as shown in **Fig. 14**(a). The equivalent mode shapes were extracted from the supermodel using the linear approximation method.

The error indicators for the ten substructures are shown in **Fig. 15**(a). It is clearly seen that the errors in both flanges and the C1 component of the cylinder are much more significant than the other components of the cylinder. The error indicator for the right flange (RL) is especially high, mainly because the inner part of the right flange has a spigot and the simplification of this feature makes the error indicator larger. The protrusion feature located on the C1 part makes the error indicator of C1 larger than the results for other components of the cylinder. The results for components C2~C8 can be considered negligible, because these components are not geometrically simplified. In order to determine the exact element of the design model at the protrusion position, the 24 elements of the C1 component were selected and the error indicators for these elements ware calculated. Because of the axial symmetry of the design model, mode shape angles exist between the design model and supermodel. For these reasons, the equivalent modal strain energy of these elements should be rearranged for every mode to match the design model. The numbers of the elements located at the protrusion position were set as 1, 2, 13 and 14. The truncated normalized error indicator for the first ten modes are shown in **Fig. 15** (b). The results show that the error is located mainly at the 1st and 13th elements, and a few modes indicate all four elements. According to the error location results, the elastic modulus of both flanges and the 1st and 13th elements of the protrusion should be updated.

As a comparison, the normalized sensitivities of the natural frequencies with respect to the elastic modulus of the ten substructures are plotted in **Fig. 16**. The elastic modulus of both flanges are the most sensitive parameters. But overall, the sensitivities of the cylinder substructures are within the same range. The conclusions drawn from the sensitivity results are obviously different from the localization results. In fact, the sensitivity analysis depends on the design model and cannot reflect the difference between the design model and the reference model. Compared with the sensitivity analysis results, these localization results are more consistent with the results of the geometric simplification.

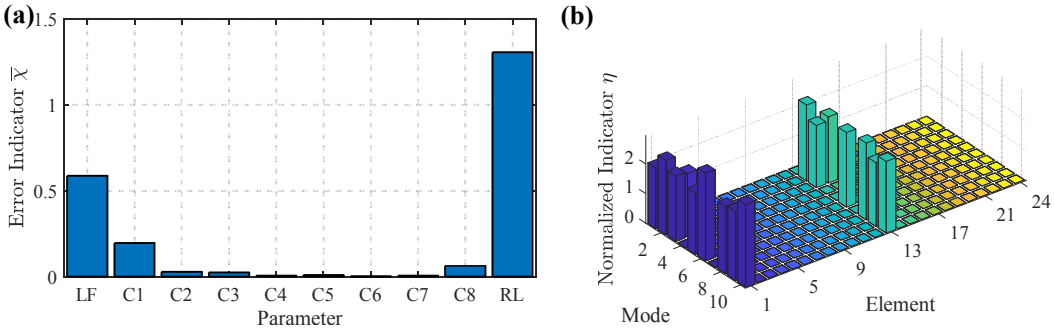

Fig. 15 Error localization for parameter selection for the casing: (a) Error localization, (b) The truncated normalized error indicator of the protrusion elements in C1

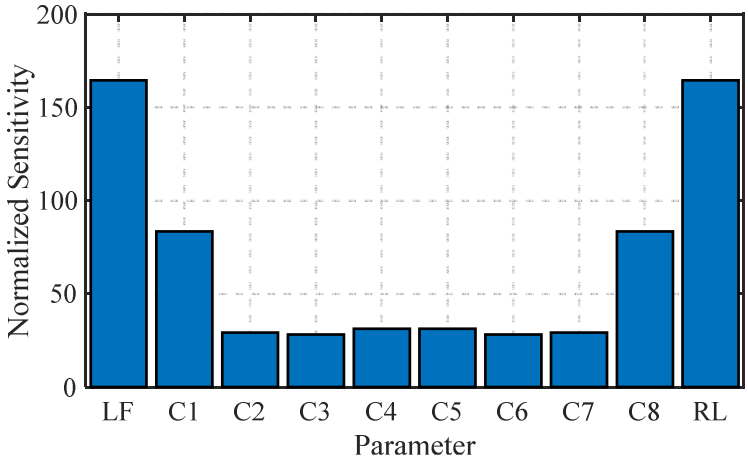

Fig. 16 Error localization for the casing based on sensitivity analysis

4.4 Model updating and results discussion

The mature model updating method based on sensitivity analysis is used here. Three parameters, namely the elastic modulus of the left flange, the right flange and the protrusion elements in C1 are selected as the updating parameters. The objective of model updating is to reduce the frequency deviation and increase the MAC values of paired modes. The correlation between the design model and the supermodel and the test data before and after model updating are shown in **Table 2**. The results clearly show that significant improvements were achieved through model updating. The maximum frequency error was reduced from 8.46% to 1.64% based on the supermodel and decreased from 8.92% to 2.79% based on the test data. The MAC value is still high. As an alternative for comparison, the elastic modulus of all the ten substructures were selected as the updating parameters. Unfortunately, the updating process did not converge satisfactorily and the updating results failed to represent the reference data.

The updating parameter changes according to the supermodel and the test data are shown in **Table 3**. These changes in the updating parameters not only reflect the errors in the model of the structure, but also the deviation in the different type of finite element model. Because of the simplification of the spigot feature and the eight bolt holes, the stiffness of this part is increased and hence parameters E_1, E_2 will decrease after model updating. The protrusion stiffness parameter, E_3, decreased after updating, mainly because the stiffness increases due to the through hole of the protrusion and the other parts of the protrusion mainly increase the additional mass rather than stiffness. The significant deviation in the correction factor E_3 is based on the different reference data, since the protrusion and the left flange are integrated in the real test structure, while in the supermodel they are not, and so the real test structure is stiffer. The results of model updating verify that the error location method can be used to effectively locate the errors in the design model.

Table 2

Comparison of natural frequency errors and the MAC before and after model updating for the casing example

Mode	Updating based on supermodel				Updating based on test data			
	Initial Error/%	Updated error/%	Initial MAC	Updated MAC	Initial Error/%	Updated error/%	Initial MAC	Updated MAC
1	8.46	0.15	0.99	0.99	8.92	-0.84	0.79	0.81
2	6.98	-0.49	0.99	0.99	8.36	-0.91	0.83	0.82
3	6.14	0.68	0.99	0.99	6.07	0.59	0.81	0.79
4	3.59	0.1	0.99	0.99	4.81	0.79	0.87	0.84
5	7.05	0.92	0.99	1.00	8.61	1.51	0.89	0.90
6	5.47	0.03	0.99	1.00	6.58	0.00	0.87	0.87
7	2.86	0.41	0.99	1.00	3.77	1.18	0.92	0.93
8	0.57	-1.64	0.99	0.99	-0.43	-2.79	0.88	0.88
9	6.21	0.24	0.99	0.99	6.46	0.14	0.96	0.89
10	4.38	-0.35	0.99	0.99	5.31	-0.10	0.84	0.89

Table 3

The correction factors of updated Young's modulus for the casing example

	Parameter	Correction factors based on supermodel/%	Correction factors based on test data/%
1	Left flange E_1	-6.59	-4.59
2	Right flange E_2	-31.97	-36.55
3	Protrusion E_3	-61.30	-47.21

For further comparison, the updating was also undertaken based on the parameter selection from the sensitivity analysis. According to **Fig. 16**, the four parameters named as LF，C1，C8，RF were first selected and the reference data were taken from the supermodel. After eight iterations the updating process converged and stabilized. **Table 4** and **Table 5** show the Young's modulus change and the frequency errors of the first ten modes before and after updating. It can be seen the model can still be updated and the maximum error in the natural frequencies is less than 1.5%. However, the Young's modulus of parameter C8 reduced by around 26%. This indicates that the updating is an inverse problem and there are no unique solutions. The selection of the parameters for updating is crucial so that the updated model is physically meaningful for real structures. Another approach is to select all ten parameters (LF, C1, …, C8, RF) as updating parameters. This updating exercise was ill-conditioned and did not converge after 50 iterations.

Table 4

The correction factors of the updated Young's modulus using the sensitivity method for localization for the casing example

Parameter	Values before and after updating	Changes /%
LF	(197,162)	-17.8
C1	(197,310)	57.4
C8	(197,146)	-25.9
RF	(197,148)	-24.9

Table 5

Comparison of the natural frequency errors and the MAC before and after model updating using the sensitivity method for localization for the casing example

No.	Supermodel	Design Model	Frequencies of Supermodel/Hz	Frequencies of design model/Hz	Frequencies error/%	MAC/ %
1	1	1	558.59	557.87	-0.13	97.87
2	2	2	566.29	557.87	-1.49	98.23
3	3	3	719.60	727.21	1.06	94.56
4	4	4	737.33	727.21	-1.37	96.99
5	5	5	1328.14	1341.27	0.99	99.07
6	6	6	1348.07	1341.27	-0.50	99.23
7	7	7	1829.93	1849.39	1.06	99.52
8	8	8	1871.64	1849.40	-1.19	99.58
9	9	10	1938.89	1956.40	0.90	97.77
10	10	9	1972.90	1956.40	-0.84	98.56

5. Conclusion

A mode shape transformation method for model error localization with modal strain energy has been presented. The supermodel is modelled with all the detailed features using solid element and the design model is built with shell elements without detailed features. Taking the supermodel as reference, the mode shape transformation from the solid elements to the shell elements is applied to obtain the equivalent mode shapes, including the rotational dofs. Based on these mode shapes, the equivalent modal strain energy can be calculated correctly and the error indicators can be established accurately and effectively to identify the model errors.

The effectiveness of the proposed mode shape transformation and error location method was demonstrated by a numerical case study of a plate structure. The numerical results show that the shape function method and the linear approximation method can both be used to

extract the equivalent mode shape data with high accuracy. The error indicator can locate the error element correctly, which is caused by simplification of protrusion and notch features. Finally, a casing structure of a rotor test rig was experimentally tested to verify the capabilities of the proposed method in engineering. The supermodel was validated using the experimental modal data and then taken as the reference for error location and model updating. The error indicator could locate the substructure of the design model which had been simplified. The updating parameter selection and model updating results based on the proposed method verified that the updating parameters are the real physical errors of the design model.

This study paves the way for the application of the error location method based on modal strain energy in the process of finite element modeling, updating and validation. The novel concept of the node displacement transformation method was proposed and it can be easily extended to solid models or other arbitrary models. With the development of full field measurement techniques, such as the continuously scanning Laser Doppler Vibrometer (CSLDV) or Laser Speckle measurement, these methods could be used based on the test data and to locate the errors in the structural model directly. Therefore, further study needs to investigate a wider range of model error types for more complex structures to improve the accuracy and applicability of the method.

Acknowledgments

The authors gratefully appreciate the financial support for this work provided by the National Natural Science Foundation of China and National Safety Academic Foundation of China (No. U1730129). The Cultivation Foundation of National Defense Large Projects of China (No. NP2018450). The support from the Jiangsu Province Key Laboratory of Aerospace Power System, the Key Laboratory of Aero-engine Thermal Environment and Structure, and the Ministry of Industry and Information Technology are also gratefully acknowledged.

References

[1] D. W. Fotsch, Development of valid FE models for structural dynamics design, PhD thesis, Imperial College, University of London, 2001.

[2] J. V. García, Development of Valid Models for Structural Dynamic Analysis, Imperial College, University of London, 2008.

[3] J.E.Mottershead, M.I.Friswell, Model updating in structural dynamics: a survey. Journal of Sound and Vibration, 167(2) (1993) 347-375.

[4] J.E.Mottershead, M.I.Friswell, Model updating in strucural dynamics, Kluwer Academic Publishers, 1995.

[5] J. E. Mottershead, M. Link, M. I. Friswell, The sensitivity method in finite element model updating: A tutorial. Mechanical Systems and Signal Processing, 25(7) (2011) 2275-2296.

[6] G.Lallement, J. Piranda, Localization methods for parameter updating of finite element models in elastodynamics. The 8th International Modal Analysis Conference, Orlando, Florida, USA, 1990.

[7] M. I. Friswell, J. E. T. Penny, S. D. Garvey, Parameter Subset Selection in Damage Location. Inverse Problems in Engineering, 5(3) (1997) 189-215.

[8] M. I. Friswell, J. E. Mottershead, H. Ahmadian, Combining Subset Selection and Parameter Constraints in Model Updating. Journal of Vibration and Acoustics, 120(4) (1998) 854-859.

[9] A. Linderholt, T. Abrahamsson, Parameter Identifiability in Finite Element Model Error Localisation. Mechanical Systems and Signal Processing, 17(3) (2003) 579-588.

[10] G.-H. Kim, Y.-S. Park, An improved updating parameter selection method and finite element model update using multiobjective optimisation technique. Mechanical Systems and Signal Processing, 18(1) (2004) 59-78.

[11] G.-H. Kim, Y.-S. Park, An automated parameter selection procedure for finite-element model updating and its applications. Journal of Sound and Vibration, 309(3-5) (2008) 778-793.

[12] G. Kim, Y.-S. Park, An improved procedure for updating finite element model based on an interactive multiobjective programming. Mechanical Systems and Signal Processing, 43(1-2) (2014) 260-271.

[13] A. Larsson, T. Abrahamsson, A comparison of error localization method in model updating. 17th International Modal Analysis Conference, Orlando, Florida, USA, 1999.

[14] M. Link, O. F. Santiago, Updating and localizing structural errors based on minimization of equation errors. International Conference on Spacecraft Structures and Mechanical Testing, Noordwijk, The Netherlands, 1991.

[15] S. W. Doebling, C. R. Farrar, M. B. Prime, D. W. Shevitz, Damage identification and health monitoring of structural and mechanical systems from changes in the vibration characteristics. Shock and Vibration, 30(5) (1996) 1-127.

[16] H. Hu, B.-T. Wang, C.-H. Lee, J.-S. Su, Damage detection of surface cracks in composite laminates using modal analysis and strain energy method. Composite Structures, 74(4) (2006) 399-405.

[17] H. Guan, V. M. Karbhari, Improved damage detection method based on Element Modal Strain Damage Index using sparse measurement. Journal of Sound and Vibration, 309(14) (2008) 465-494.

[18] H. Hu, C. Wu, Development of scanning damage index for the damage detection of plate structures using modal strain energy method. Mechanical Systems and Signal Processing, 23(2) (2009) 274-287.

[19] H. Hu, C. Wu, W.-J. Lu, Damage detection of circular hollow cylinder using modal strain energy and scanning damage index methods. Computers & Structures, 89(1-2) (2011) 149-160.

[20] W. Fan, P. Qiao, A strain energy-based damage severity correction factor method for damage identification in plate-type structures. Mechanical Systems and Signal Processing, 28(1) (2012) 660-678.

[21] R. J. Guyan, Reduction of stiffness and mass matrices. AIAA Journal, 3(2) (1965) 380-380.

[22] J. O'Callahan, A Procedure for an Improved Reduced System (IRS) Model. 7th International Modal Analysis Conference, Las Vegas, Nevada, USA, 1989.

[23] M. I. Friswell, S. D. Garvey, J. E. T. Penny, Model Reduction Using Dynamic and Iterated IRS Techniques. Journal of Sound and Vibration, 186(2) (1995) 311-323.

[24] J. O'Callahan, P. Avitabile, R. Riemer, System Equivalent reduction Expansion Process. 7th International Modal Analysis Conference, Las Vegas, Nevada, USA, 1988.

[25] H.-P. Chen, Mode shape expansion using perturbed force approach. Journal of Sound and Vibration, 329(8) (2010) 1177-1190.

[26] F. Liu, Direct mode-shape expansion of a spatially incomplete measured mode by a hybrid-vector modification. Journal of Sound and Vibration, 330(18-19) (2011) 4633-4645.

[27] F. Liu, H. Li, Rapid direct-mode shape expansion for offshore jacket structures using a hybrid vector. Ocean Engineering, 51(1) (2012) 119-128.

[28] F. Liu, H. Li, A two-step mode shape expansion method for offshore jacket structures with physical meaningful modelling errors. Ocean Engineering, 63(1) (2013) 26-34.

[29] M. Petyt, Introduction to Finite Element Vibration Analysis Second Edition, Cambridge University Press, 2010.